The EMBO Journal Vol. 22 No. 23 pp. 6182–6192, 2003

Structure of the mitochondrial ATP synthase by electron cryomicroscopy

John L.Rubinstein[1,2,3], John E.Walker[4] and Richard Henderson[1]

[1]MRC Laboratory of Molecular Biology, Hills Road, Cambridge CB2 2QH and [4]MRC Dunn Human Nutrition Unit, Hills Road, Cambridge CB2 2XY, UK

[3]Present address: Banting and Best Department of Medical Research, University of Toronto, 112 College Street, Toronto, Ontario M5G 1L6, Canada

[2]Corresponding author
e-mail: john.rubinstein@utoronto.ca

We have determined the structure of intact ATP synthase from bovine heart mitochondria by electron cryomicroscopy of single particles. Docking of an atomic model of the F_1-c_{10} subcomplex into a major segment of the map has allowed the 32 Å resolution density to be interpreted as the F_1-ATPase, a central and a peripheral stalk and an F_O membrane region that is composed of two domains. One domain of F_O corresponds to the ring of c-subunits, and the other probably contains the a-subunit, the transmembrane portion of the b-subunit and the remaining integral membrane proteins of F_O. The peripheral stalk wraps around the molecule and connects the apex of F_1 to the second domain of F_O. The interaction of the peripheral stalk with F_1-c_{10} implies that it binds to a non-catalytic α–β interface in F_1 and its inclination where it is not attached to F_1 suggests that it has a flexible region that can serve as a stator during both ATP synthesis and ATP hydrolysis.

Keywords: ATP synthase/electron microscopy/single particle/three-dimensional structure

Introduction

The mitochondrial adenosine triphosphate synthase (ATP synthase) is a membrane-bound multisubunit enzyme that couples the proton motive force across the inner mitochondrial membrane to the synthesis of ATP in the matrix (Boyer, 1997; Walker, 1998). The bovine complex contains 16 different proteins (including the regulatory subunit, IF_1) and has a mass of ~600 kDa (Walker *et al*., 1991). The extramembranous F_1 catalytic subcomplex is attached to the membrane intrinsic F_O subcomplex by a central stalk and a peripheral stalk (Walker, 1998). As protons pass through the membrane domain, a rotational force is generated in F_O between the ring of c-subunits and the a-subunit. The rotational force causes the entire central rotor, the γδε-c_{10} subcomplex, to turn (Sambongi *et al*., 1999; Stock *et al*., 1999; Pänke *et al*., 2000) and drives the synthesis of ATP in the $\alpha_3\beta_3$ subcomplex of F_1. The enzyme can also catalyse the reverse reaction, with ATP hydrolysis in F_1 driving proton pumping in F_O. The peripheral stalk acts as a stator that prevents the $\alpha_3\beta_3$ subcomplex from following the rotation of the central stalk. Consistent with this role, the peripheral stalk can be cross-linked to an α-subunit without preventing rotation of the rotor (Ogilvie *et al*., 1997).

The peripheral stalk is composed of single copies of the oligomycin sensitivity conferral protein (OSCP) and subunits b, d and F_6 (Collinson *et al*., 1994a, 1996). Residues 1–10 of OSCP (Joshi *et al*., 1996) interact with residues 1–15 of one or more α-subunits and with residues 1–5 of one or more β-subunits that are located at the top of F_1 distal from F_O (Hundal *et al*., 1983; Dupuis and Vignais, 1985; Walker *et al*., 1985; Abrahams *et al*., 1994). The OSCP extends almost 100 Å along the surface of F_1 towards F_O (Rubinstein and Walker, 2002). A C-terminal segment of OSCP interacts with the C-terminal domain of subunit b (Joshi *et al*., 1996), which continues towards the membrane. Subunits d and F_6 both interact with subunit b (Collinson *et al*., 1994a). Residues 20–80 of subunit b probably form two transmembrane helices joined by a hydrophilic loop that protrudes into the intermembrane space (Walker *et al*., 1987). Since the OSCP-bdF_6 subcomplex was proposed to form a separate domain and play the role of a stator (Walker, 1998), the peripheral stalk has been observed by electron microscopy (EM) in the isolated enzyme from various species (Böttcher *et al*., 1998; Wilkens and Capaldi, 1998a; Karrasch and Walker, 1999).

The structures of several subcomplexes of ATP synthase have been determined by X-ray crystallography, most notably the F_1-ATPase ($\alpha_3\beta_3\gamma\delta\varepsilon$) from the bovine enzyme (Gibbons *et al*., 2000), the F_1-c_{10} subcomplex ($\alpha_3\beta_3\gamma\delta\varepsilon$-$c_{10}$) from the yeast *Saccharomyces cerevisiae* (Stock *et al*., 1999) and the F_1-ATPase ($\alpha_3\beta_3\gamma$) from spinach chloroplasts (Groth and Pohl, 2001). The structure of the bovine inhibitor protein, IF_1, has also been determined in isolation (Cabezón *et al*., 2001) and in complex with the F_1-ATPase (Cabezón *et al*., 2003). In addition, the structures of several individual subunits and fragments of subunits have been solved by solution NMR spectroscopy. They include residues 1–105 of the *Escherichia coli* δ-subunit (Wilkens *et al*., 1997), residues 1–120 of the homologous bovine OSCP (R.J.Carbajo, F.A.Kellas, M.J.Runswick, J.E.Walker and D.Neuhaus, manuscript in preparation), the bovine F_6-subunit (R.J.Carbajo, J.A.Silvester, M.J.Runswick, D.Neuhaus and J.E.Walker, manuscript in preparation), and residues 1–34 (Dmitriev *et al*., 1999) and 62–122 (Del Rizzo *et al*., 2002) of the *E.coli* b-subunit. However, there is still little information about how the subunits of the peripheral stalk interact with each other and with the F_1 and F_O regions of the enzyme.

In this paper, we present images of the ATP synthase obtained by electron cryomicroscopy (cryoEM) of single

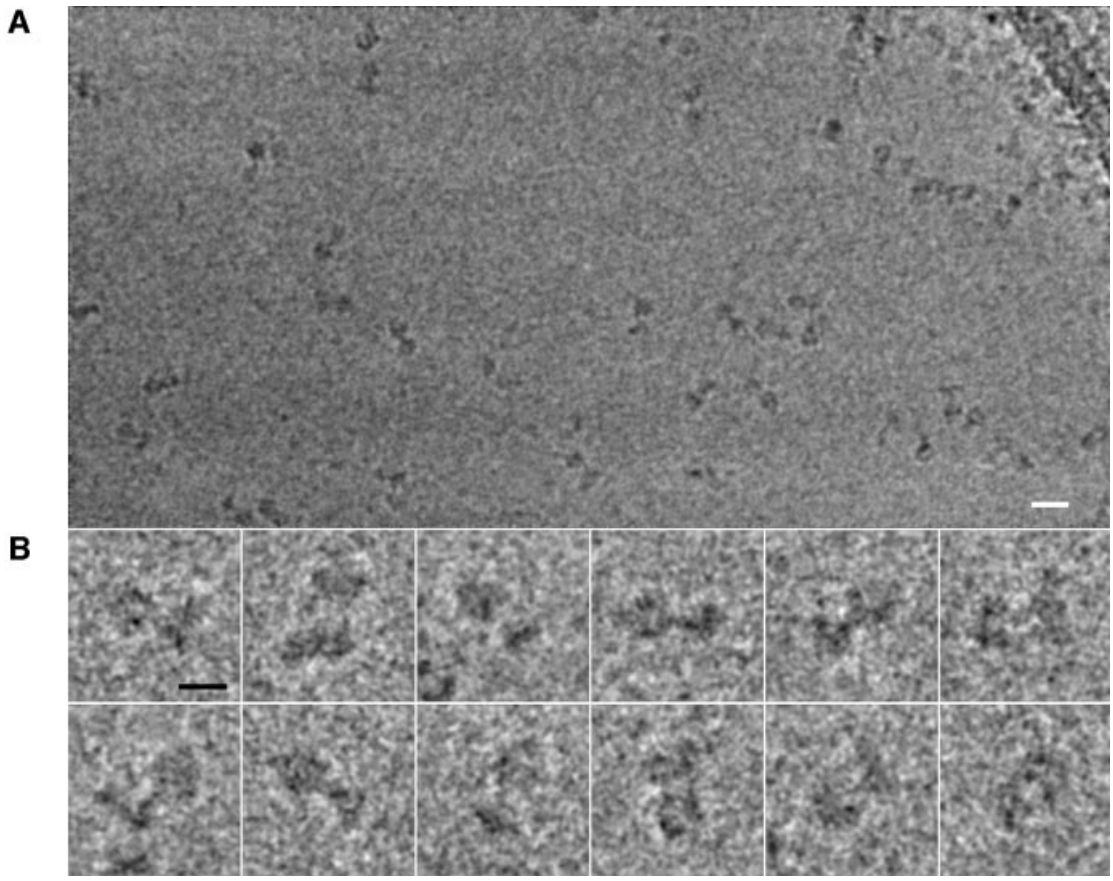

Fig. 1. EM of ATP synthase particles. Frozen ATP synthase particles were imaged with a 200 kV electron microscope. (**A**) A sample region from a micrograph. (**B**) Some typical particle images. The scale bar in (A) represents 200 Å and the scale bar in (B) represents 100 Å.

particles. Class-averages derived from multivariate statistical analysis of these images reveal new structural information about both the F_O membrane region and the peripheral stalk, and we provide evidence that these class-averages are authentic projected views of the complex. Using a new procedure, the views were placed in a sequence to form a 'movie' showing the complex as it is rotated about its long axis. The projected views of the structure were used to construct and refine a 3-D model for the ATP synthase that differs significantly from previously proposed models. An atomic model of the F_1-c_{10} subcomplex has been docked unambiguously into a major segment of the EM map. This docking allows clear identification of the remaining density corresponding to the peripheral stalk and attached second domain in the F_O membrane region. The structure suggests how the stator functions and provides significant restraints on the subunit organization in the F_O region of the complex.

Results

Electron microscopy of the ATP synthase

Using cryoEM, the bovine ATP synthase was imaged unstained in vitreous ice in holes in a perforated carbon support attached to a copper EM grid (Figure 1A). The images of the ATP synthase are, in general outline, similar to those obtained for the negatively stained molecule from a variety of sources (Böttcher *et al*., 1998; Wilkens and Capaldi, 1998a; Karrasch and Walker, 1999; Rubinstein and Walker, 2002). The images show two globular regions of different size connected by a central stalk. In most images, the globular F_1 could be distinguished readily from the smaller, flatter, F_O but it was not possible to identify the peripheral stalk unambiguously (Figure 1B).

A dataset of 5984 particle images was aligned, subjected to multivariate statistical analysis (van Heel *et al*., 1996) and separated into 20 classes. Figure 2A shows the average of all 5984 particle images after alignment and Figure 2B–U shows the class-averages. In contrast to the strong orienting forces exerted on particles when they are attached to a continuous carbon support, particles in the thin film of buffer in a hole in a perforated carbon support are relatively free to adopt any orientation. However, there is a predominance of class-averages where the long axis of the complex lies almost parallel to the support. This observation indicates that either the thickness of the buffer film is less than the particle height of ~200 Å or that there is some interaction between the particles and the air–water interface. Some portion of the thickness of the buffer film must be taken up by a monolayer of detergent at each air–water interface of the film, further reducing the height available to the protein particles.

The presence of mirror-image pairs in the class-averages can help to distinguish bona fide views of the particle from possibly artefactual class-averages that result

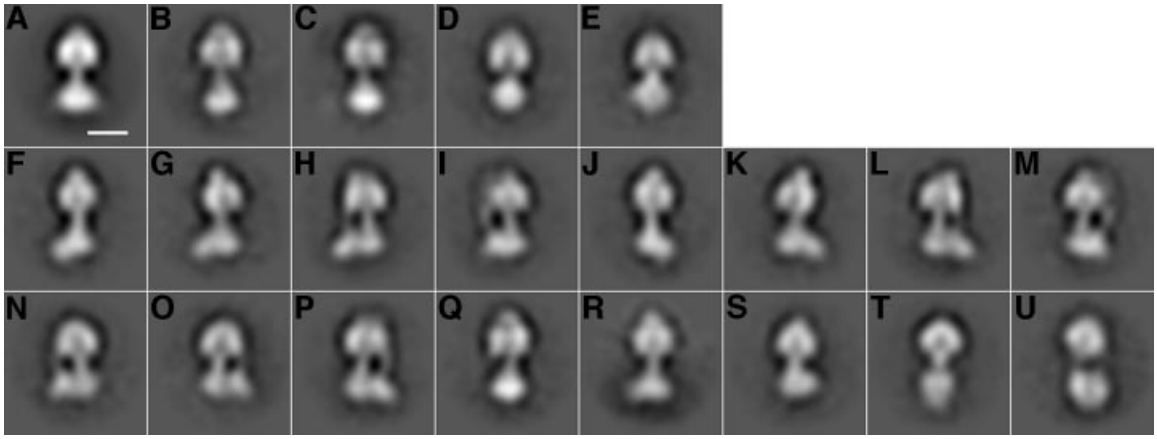

Fig. 2. Class-average images of the ATP synthase. (**A**) Average of all of the aligned images in the dataset. The scale bar represents 100 Å. (**B–E**) Class-averages that probably arise from incoherently averaged particle images (and consequently, like the overall average, have a line of symmetry). (**F–M**) Class-averages where a corresponding mirror image is found (e.g. F with J, G with K, etc.) and constitute views about the long axis of the complex. (**N** and **O**) A mirror pair, but each probably consisting of averages of two non-equivalent views of the assembly with the long axis tilted from the plane of the grid. (**P–U**) Class averages that have no mirror pair in the dataset.

from averaging non-equivalent or misaligned images. The two air–water interfaces of the buffer film should be indistinguishable from the point of view of the ATP synthase molecules. Therefore, if there were any interactions between the particle and the interfaces, an equal number of particles would be expected to interact with each interface. In the electron micrographs, particles interacting equivalently with opposite air–water interfaces would appear in projection as mirror images of each other. The consequence of this logic is that, whether or not there are interactions with air–water interfaces producing preferred orientations, mirror-image pairs in the class-averages should occur for authentic views. Indeed, even though images were never mirrored in the data analysis process, there exist 10 class-averages (F–O) that appear to have a mirror-image class-average in the data set (e.g. F with J, G with K, etc.). Class-averages F–M have the same overall length and are views of the particle where its long axis is parallel to the plane of the EM grid. In several of these views (H, I, L and M), the peripheral stalk of the complex is apparent. The nature of views F, G, J and K, where the peripheral stalk does not form a visible feature, cannot be interpreted sensibly without considering the 3-D structure of the enzyme and will be discussed later. The asymmetry of the F_O region of the complex is also evident, and in class-averages G, H, K and L, F_O appears to consist of two domains.

The class-averages in the mirror pair of N and O are shortened relative to F–M, as if the long axis of the complex is not perfectly parallel to the plane of the grid. However, there are two non-equivalent ways in which the long axis of the complex can be tilted from the plane of the grid that would result in the same extent of shortening. Therefore, it is likely that both images N and O consist of a mixture of non-equivalent out-of-plane views.

In contrast, several class-averages have no mirror images (Figure 2P–U). These class-averages should be interpreted with caution as they may be artefactual. Other class-averages (Figure 2B–E) appear to have a mirror line of symmetry. These symmetric class-averages are similar to the average of all of the images in the data set (Figure 2A) and therefore may also not correspond to views of the complex. Mirror lines are likely to arise by incorrectly classifying together and incoherently averaging particle images that actually consist of +90° and –90° rotations about an axis parallel to the grid. Consequently, the average of the class is symmetric, just as the average of all of the images in the data set is symmetric. The models proposed by several others (Wilkens, 2000; Mellwig and Böttcher, 2001; Mellwig and Böttcher, 2003) have incorporated mirror-symmetric class-averages as views, and thus may have forced the 3-D model to have a mirror plane of symmetry.

It is important to note that the mirror-image logic does not apply to the case of particles attached to a carbon support. In that instance, the buffer layer has a unique air–water interface and a unique carbon–water interface, so that asymmetric views without a corresponding mirror-symmetric view may occur.

Considering the significant asymmetry apparent in our side-views of ATP synthase, the question arises as to why such asymmetric views have not been apparent in the previously published images of the negatively stained complex. To answer this question, we prepared samples where ATP synthase particles were allowed to adsorb to a thin continuous carbon support, briefly rinsed and then vitrified (results not shown). This protocol mimics experiments done previously with negative stain, except that the frozen hydrated protein can be compared directly to our results for frozen hydrated ATP synthase in holes in a perforated carbon support-covered grid. After image analysis, it became apparent that adsorption to the carbon support introduced a further degree of preferred orientation to the particles. Mirror pairs in the class-averages did not exist for this set of images. No views were found where the domains of F_O could be clearly observed or where the portion of the peripheral stalk that interacts with F_1 did not overlap with F_1. This strongly preferred orientation, with the peripheral stalk always on one side of the projection map, has been reported previously (Karrasch and Walker,

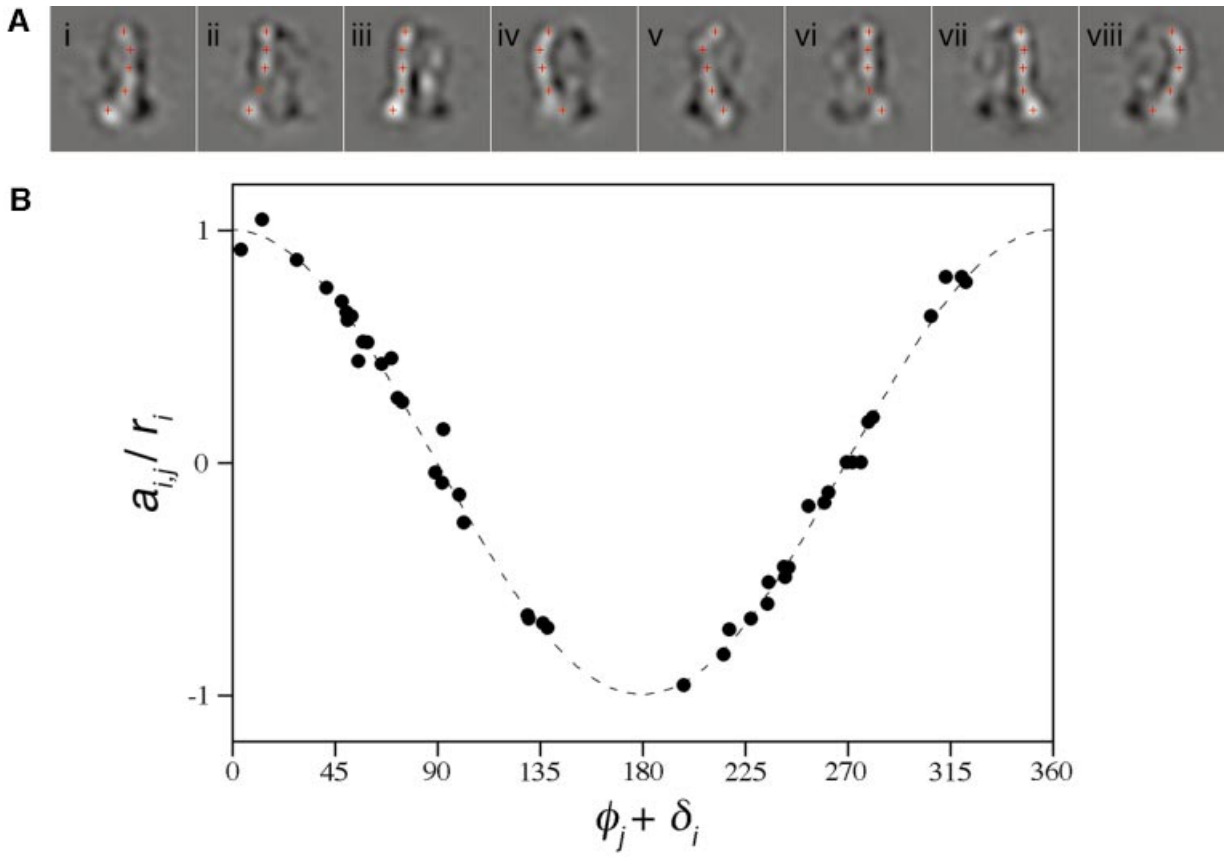

Fig. 3. Rotation analysis. (**A**) Features that deviated from cylindrical symmetry in class-averages of Figure 2F–M were emphasized by subtracting the average of all of the views from each of the views. Markers were placed at maxima in the density to indicate the corresponding asymmetric features in each image. (**B**) To compare the experimental marker positions to the hypothesis that the images of the ATP synthase constitute a single-axis rotation series, the ratio of marker position to calculated marker radius ($a_{i,j}/r_i$) was plotted against the total angle for each marker in each image ($\phi_j + \delta_i$). The observations are consistent with the hypothesis that the series constitutes a rotation sequence, indicated by the dashed line ($\cos[\phi_j + \delta_i]$).

1999). Our observations offer a possible explanation for the limited orientations observed on continuous carbon supports. We cannot explain why Mellwig and Böttcher (2003), using perforated carbon, did not observe side-views showing two domains of F_O in the chloroplast ATP synthase.

Views of the complex arranged into a rotational sequence

Class-averages in Figure 2F–M appear to constitute a single-axis rotation series with the rotation axis parallel to the *y*-axis of each image. This situation is similar to a tomographic series, but with unknown relative tilt angles. The common lines or angular reconstitution algorithms (Crowther *et al*., 1970; van Heel, 1987) are frequently used to determine the relative orientations of views of a molecule. However, for these methods to define the relative orientation of two views about their common line, a third view is required that does not share the common line with the pair. The Fourier transforms of the different side-views of the ATP synthase all share a single common line and the algorithm has no information that can be used to determine the orientations of the views about the long axis of the complex. Consequently, an initial model prepared by the common lines method could easily be based on incorrectly assigned projection angles, with the result that any signal deviating from the cylindrical average would be likely to be incorrect. With the current generation of projection matching EM structure refinement software, which tend to reinforce the initial model (Sigworth, 1998), it is important to begin structure refinement with a correct model.

Rather than using a common lines method, we developed a method to test the hypothesis that the views represent a rotation series and, if verified, assign the relative orientation of each view about the axis. This method uses asymmetric features in the images as fiducials for determining the direction of projection. To emphasize the features in class-averages F–M that deviate from cylindrical symmetry, the average of all of the views was subtracted from each of the views. The remaining density, shown in Figure 3A, results from the asymmetric features in the structure. In these difference maps, this density can be seen as a continuous feature arising from the peripheral stalk of the complex. The feature starts at the top of F_1 and ends as a domain in F_O, and can even be seen in projections where it overlaps with the central stalk (Figure 3A, parts i, ii, v and vi). In Figure 3A, parts ii and vi, the feature decreases in intensity from its overlap with the negative signal created by the effect of the contrast transfer function of the microscope on the central stalk and edges of F_1 and F_O. Although the existence of a third stalk, that is a second

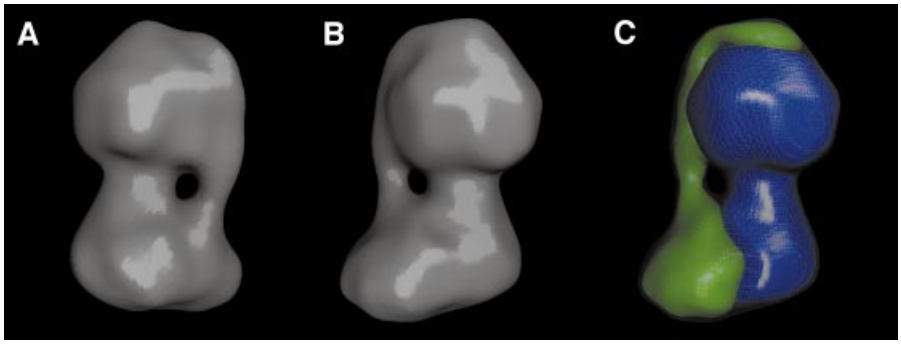

Fig. 4. 3-D model of the ATP synthase. (**A** and **B**) Surface rendered views of the model after refinement. (**C**) The model after being divided into two parts. The first (blue) was chosen to correspond to the F_1-c_{10} subcomplex and the remaining density (green) is interpreted to represent the peripheral stalk and second domain of F_O. The grey mesh represents the experimental EM map.

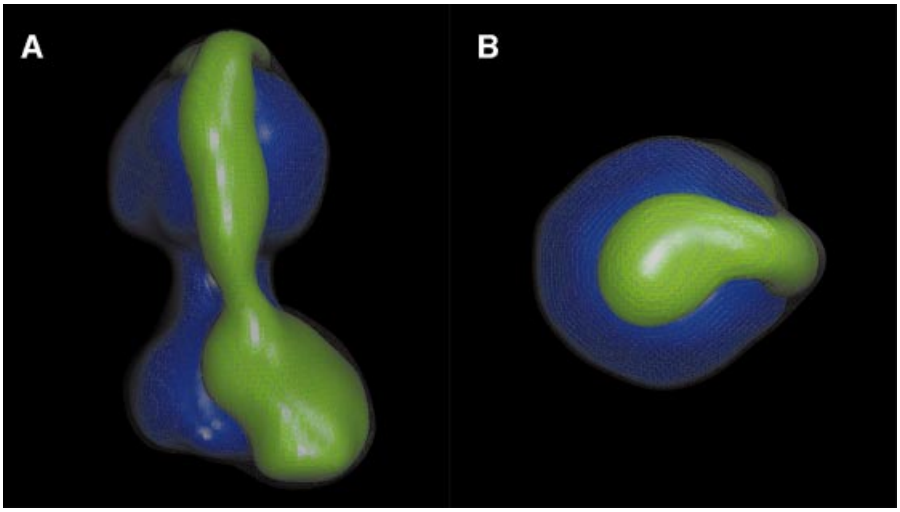

Fig. 5. Two further views of the peripheral stalk. (**A**) A side-view of the model shows the curvature of the peripheral stalk. (**B**) A view from the F_1 end of the assembly along its long axis reveals a sharp bend in the peripheral stalk near to its terminus.

peripheral stalk, has been proposed for the *E.coli* enzyme (Böttcher *et al*., 2000), from Figure 3A it is clear that there is only one peripheral stalk in the bovine mitochondrial enzyme.

For a projection from a single-axis rotation series, the displacement, a, of a feature from the central vertical line of the image is given by:

$$a = r_{feature}\cos(\phi_{projection} + \delta_{feature})$$

where $r_{feature}$ is the radial distance between the feature and rotation axis, $\phi_{projection}$ is the angle of projection about the rotation axis and $\delta_{feature}$ is the relative angular offset of different features.

As shown in Figure 3A, several markers were placed at maxima in the density at the same values of y in different images. The markers indicate the corresponding asymmetric features in the images. A conjugate gradient minimization method was used fit a value of ϕ for each image and r and δ for each marker. The output values of ϕ were 57, 38, 20, 274, 238, 210, 195 and 98° for images in Figure 2F–M. As an internal check on consistency, it can be seen that views that are approximate mirror images of each other have ϕ values that are ~180° apart: 181° for F and J, 172° for G and K, 175° for H and L, and 176° for I and M. The asymmetric class-average from Figure 2P also conformed to the rotational model (at ϕ = 186°) and was therefore included in the analysis. It is possible that the 847 particle images contributing to class-averages L, P and M have been separated more successfully than the 896 images contributing to H and I.

In Figure 3B, the ratio of $a_{i,j}/r_i$ was plotted against (ϕ_j + δ_i) for each marker, where j denotes the image and i indicates the feature. Because each marker position was measured from the centre of each image, $a_{i,j}$ is the projection of a vector length r_i on the x-axis and, if the set of images is a rotation series, the ratio $a_{i,j}/r_i$ should be the cosine of the angle (ϕ_j + δ_i). A value on the x-axis of 0 or 360° indicates that a marker is at one extreme of its displacement from the central line of the image while 180° indicates that it is at the other extreme. The dashed line gives the hypothesis (cosine of the angle) that the images constitute a single-axis rotation series. From Figure 3B, it can be seen that the data are consistent with the rotation hypothesis (coefficient of determination, R^2 = 0.990).

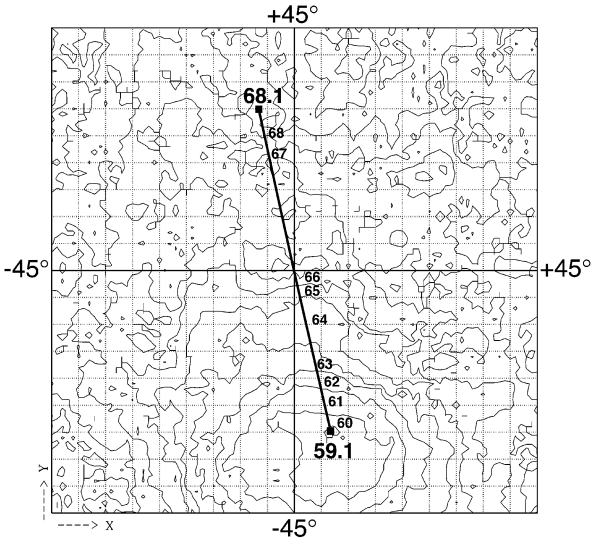

Fig. 6. Determination of the absolute hand of the model. Tilt pairs of 29 different particles were recorded with a tilt between images of 30°. The first particle in each pair was aligned to the model. The plot shows the average phase residual between the model and the second particle in each pair for all possible tilt axes and tilts up to 40°. From the known direction and magnitude of the tilt between the images in the pair, a model of the correct hand was expected to produce a minimum at (2,–30°) as opposed to (–2,30°). The observed tilt axis and amount of tilt indicate that the model, as shown, is correct.

Images in the rotational sequence were combined to make a 'movie' that gives the impression of the ATP synthase complex being rotated about its vertical axis (see Supplementary data available at *The EMBO Journal* Online or www2.mrc-lmb.cam.ac.uk/VA/Rubinstein/ATP_Synthase1.html). The 'movie' shows the two-domain structure of F_O. It also reveals that the peripheral stalk is curved and wraps around the complex as it traverses the distance from the top of F_1 to F_O. It is apparent both from the rotational sequence and the difference maps in Figure 3 that in Figure 2F, G, J and K, the curved peripheral stalk is not missing, but is simply hidden by the central stalk. ATP_Synthase2.html shows the movement of marker positions used in the rotational analysis.

The 3-D structure of the ATP synthase

The ϕ angles obtained by fitting class-averages to the rotation hypothesis were used to generate a 3-D model of the ATP synthase (θ = 90°), which was then iteratively refined by projection matching. By the 0.143 threshold criteria for the Fourier shell correlation (Rosenthal *et al*., 2003), the resolution of the model was determined to be ~32 Å. The peripheral stalk and the two domains of F_O can be seen in surface rendered views of the EM map (Figure 4A and B). Since the shape of the density in the right-hand portion of Figure 4B strongly resembles the shape of the F_1-c_{10} subcomplex determined by X-ray crystallography, we divided the experimental density into two segments using minima found in sections of the map to guide the partition. One segment consists of the peripheral stalk and second domain of F_O and the other corresponds to the F_1-c_{10} subcomplex (Figure 4C). In the model, the two domains of F_O are of nearly equal volume. Other views of the partitioned model reveal the curvature of the peripheral stalk and a sharp bend near to its terminus at the central axis of F_1 (Figure 5).

Several studies have observed the presence of a cap structure at the top of F_1 (Wilkens and Capaldi., 1998b; Karrasch and Walker, 1999; Böttcher *et al*., 2000; Mellwig and Böttcher, 2003), although in one (Böttcher *et al*., 2000) the structure was reported to be evident only when the ATP synthase was inhibited with the non-hydrolysable ATP analogue AMP-PNP and not in the absence of this inhibitor. In these earlier studies, the cap appears as a structure sitting on top of F_1 but disconnected from the peripheral stalk. In our model, the peripheral stalk is a continuous structure. However, since it is curved, there are several projections of the structure where the terminus is visible above F_1, but the rest overlaps with F_1 and the central stalk, giving the appearance of a cap. These views are seen in Figure 2F, G, J and K.

As with any EM map built from untilted micrographs, the absolute hand of the map was initially unknown and arbitrarily chosen. Using a pair of tilted images recorded from the same field of particles and an automatic method (Rosenthal and Henderson, 2003), we tested the model to see if it is of the correct or incorrect hand. This procedure is known to be robust from its application to cases where the correct hand of the structure was already known. The plot in Figure 6 shows that the known magnitude and direction of the relative tilt between the pair of images can be determined independently by aligning particle images to the 3-D model. The location of the minimum indicates that the model is of the correct hand. The tilt experiment is also an entirely objective test of the structure: it provides further proof that the model is substantially correct and justifies the angular determination method described above.

Based on the crystal structure of the F_1-c_{10} complex from *S.cerevisiae* (Stock *et al*., 1999) we assembled a model of F_1-c_{10} consisting of the bovine F_1-ATPase (Gibbons *et al*., 2000) and an oligomer of 10 *E.coli* c-subunits (Girvin *et al*., 1998; Stock *et al*., 1999). The number of c-subunits seems to vary in ATP synthase isolated from different organisms (Stock *et al*., 1999; Seelert *et al*., 2000; Stahlberg *et al*., 2001). The resolution of our EM data is insufficient to determine the number of c-subunits in the bovine enzyme. Consequently, the oligomer of 10 c-subunits was based on the stoichiometry observed in the yeast F_1-c-ring assembly, the most intact complex for which a definitive structure is known. The F_1-c_{10} structure was manually docked into the EM map (Figure 7). The EM map has several flattened sides that match the six flattened sides of the F_1-ATPase crystal structure. These surfaces constrain the choice of orientation of F_1-c_{10} to six positions in the EM map differing by 60° rotations about the long axis of the subcomplex (Figure 7B and C). The three catalytic α–β interfaces and the three non-catalytic interfaces create flattened sides with different dimensions. Although we do not think that it is possible to distinguish the α- from the β-subunits with complete certainty, the model shown gives the most likely orientation of the F_1-c_{10} subcomplex within the map. It is apparent that along most of its contact region with F_1, the peripheral stalk runs approximately along an α–β interface

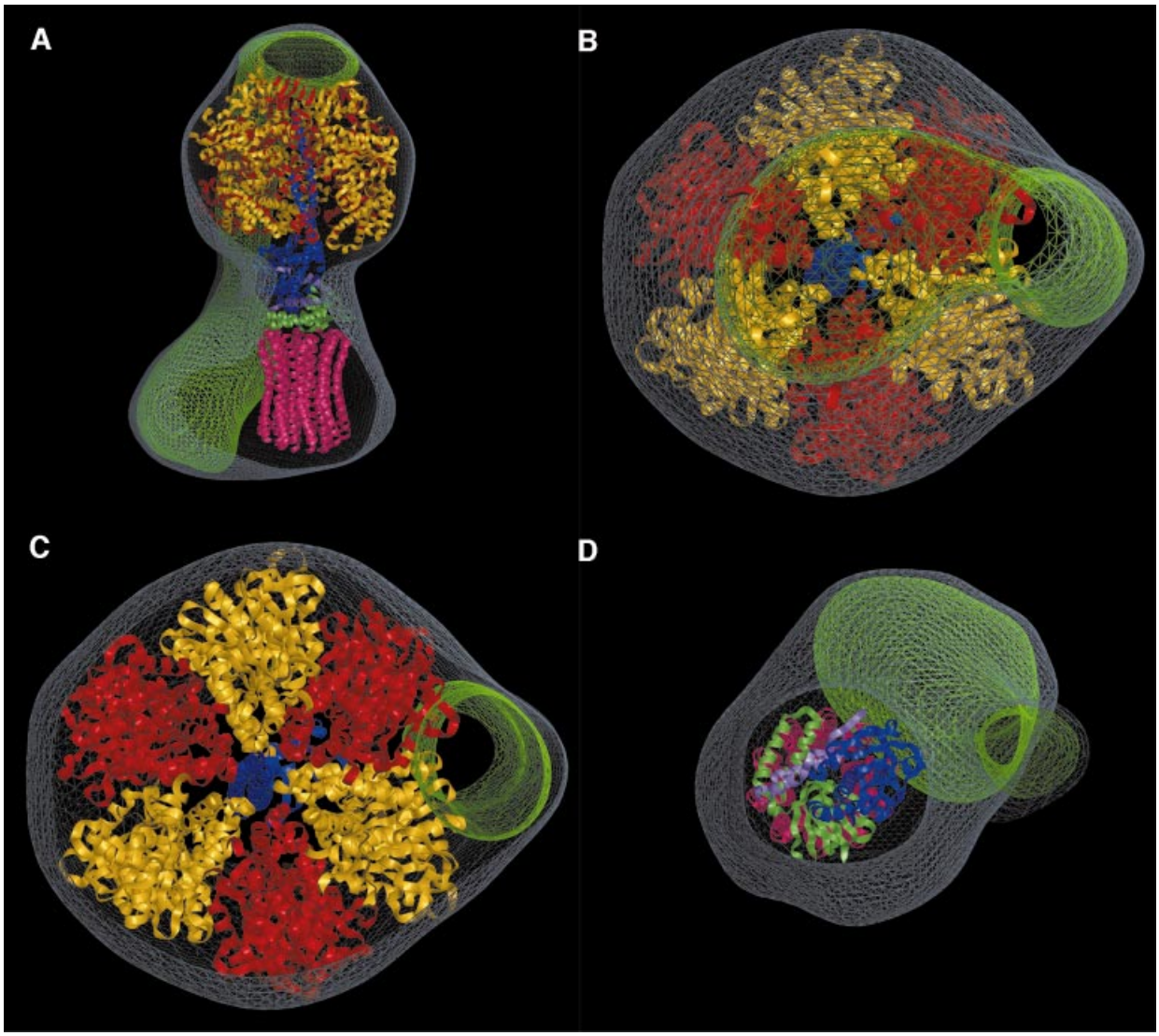

Fig. 7. Docking of an atomic model of F_1-c_{10} into the EM map. The volume of the EM map not occupied by the atomic structure is coloured green. (**A**) A side-view of the model. The density that cannot be explained by the F_1-c_{10} model consists of the peripheral stalk and the second domain of the F_O region. This density must contain the remaining subunits of the ATP synthase: a, b, d, e, f, g, A6L, F_6 and OSCP. (**B–D**) Cross-sections of the model. The terminus of the peripheral stalk at the top of F_1 is on the central axis at the apex of the model (B). The peripheral stalk is primarily in contact with an α-subunit (red) near the top of F_1, but is in contact with a non-catalytic interface between an α- (red) and β- (yellow) subunit along most of F_1. The matching flattened sides of the F_1 in the crystal structure and EM map show the uniqueness of fit between the two models. The central stalk and c-ring fit into the model well (D).

(red and yellow, respectively). In our docking, the peripheral stalk contacts a non-catalytic interface, leaving all three catalytic interfaces accessible. At the top of F_1, the peripheral stalk is in contact almost entirely with an α-subunit. The modelled c_{10}-ring appears to be smaller than the size of the c-ring domain in the EM map. This discrepancy may be the result of bound lipids that contribute to the size of the c-ring domain in the intact complex, a stoichiometry of more than 10 subunits in the bovine enzyme, or averaging of different conformations of the c-ring that leads to blurring and an exaggeration of its size in the EM map.

Discussion

The F_1-c_{10} subcomplex contains 6 of the 16 different subunits of ATP synthase and accounts for 75% of its calculated mass. By dividing the model into the segment containing the known F_1-c_{10} structure and the segment containing the other subunits, we found that the F_1-c_{10} accounts for 78% of the model volume at the chosen threshold value. In the F_1 region, the map agrees well with the atomic model, with the exception of the N termini of the α-subunits, which are known to interact with OSCP and are probably not in their native conformation in the crystal structure of the F_1-ATPase.

The asymmetric central rotor of ATP synthase has the ability to rotate 360° relative to the stator. Consequently, a population of ATP synthase assemblies is likely to contain a heterogeneous mixture of conformations of the inherently asymmetric F_1 region and a variety of positions of the central rotor with respect to the stator. The presence of a heterogeneous population of particles containing different rotational positions of the rotor could explain why the

resolution of the structure presented here is ~32 Å. It may be possible to separate images of the ATP synthase particles in different conformations by computation and so achieve a higher resolution for each structure.

The peripheral stalk

The defined location of the peripheral stalk indicates a degree of specificity in its interaction with the surface of F_1. The N terminus of the OSCP binds to the N-terminal regions of the α-subunits, which are on the top of F_1 (Hundal *et al*., 1983; Abrahams *et al*, 1994; Joshi *et al*., 1996). In the yeast enzyme, the C terminus of the OSCP extends almost 100 Å along the surface of F_1 (Rubinstein and Walker, 2002). In the present model, the terminus of the peripheral stalk sits on the apex directly above the central axis of the F_1-c_{10} and the peripheral stalk itself has a sharp bend ~20 Å from the top of F_1 (Figure 5B). Together, these observations indicate that in ATP synthase, OSCP has a kinked structure, with the N-terminal domain (residues 1–118) probably occupying the region of the peripheral stalk from the central axis of F_1 to the sharp bend. This unique central position explains how the asymmetric OSCP binds to a single site on the pseudo-3-fold-symmetric F_1 region. The peripheral stalk is in contact mainly with one α-subunit near the top of F_1 and runs along a non-catalytic α–β interface on the side of F_1. This position is consistent with cross-linking studies of the *E.coli* enzyme that show that the b-subunit can be cross-linked to both an α- and a β-subunit at a non-catalytic interface on the side of F_1, but only to an α-subunit near to the top of F_1 (McLachlin *et al*., 2000) and that the δ-subunit (equivalent to OSCP) cross-links to an α-subunit (Ogilvie *et al*., 1997).

Current understanding of the rotary mechanism of the ATP synthase suggests that in order to match the 3-fold symmetry of $\alpha_3\beta_3$ to the 10-fold symmetry of the c-ring, the enzyme must undergo elastic distortions in both the central rotor and peripheral stalk (Junge *et al*, 1997; Cherepanov *et al*., 1999; Stock *et al*., 1999; Ma *et al*., 2002). In the *E.coli* ATP synthase, the b-subunit forms a homodimer and is a major component of the peripheral stalk. Mutational studies of a domain consisting of residues 23–53 show that the enzyme can tolerate insertions or deletions of up to 14 and 11 residues, respectively, and functions essentially as wild-type with insertions or deletions of up to seven residues (Sorgen *et al*., 1998,1999). These experiments indicate that the peripheral stalk, particularly in this domain, has an inherently flexible structure that is better viewed as an elastic rope rather than a rigid rod. It has been suggested that flexibility of the domain might allow reorientation of the stalk to act as a stator for rotation in one direction during ATP synthesis and the opposite direction during ATP hydrolysis (Grabar and Cain, 2003). In our model, the peripheral stalk has a change in inclination between the region in contact with an α–β interface and the region that is not attached to F_1. From this bend, we suggest that the flexible domain of the peripheral stalk is located between the second domain of F_O and the α–β interface.

The inclination of the flexible domain of the peripheral stalk can be considered in terms of the likely function of the peripheral stalk. We observe from our data that the peripheral stalk wraps around the ATP synthase with a left-handed curve. This orientation of the peripheral stalk in our model is consistent with the state of the sample. When viewed from the F_O end of the complex towards F_1, the rotor ($c_{10}\gamma\delta\varepsilon$) turns in a clockwise direction when synthesizing ATP and a counter clockwise direction when hydrolysing ATP (Abrahams *et al*., 1994; Noji *et al*., 1997). In our preparation of ATP synthase, ATP synthesis activity was abolished at the beginning of the purification protocol when the proton motive force was dissipated by disruption of the mitochondria. In the absence of the bound inhibitor protein, hydrolysis of the available ATP would have immediately ensued and adding an excess of ADP would have trapped the enzyme in an ATP hydrolysing conformation. Consequently, the peripheral stalk would wrap around the $\alpha_3\beta_3$ subcomplex with the observed left-handed twist as required to prevent the $\alpha_3\beta_3$ from following the rotation of the rotor during hydrolysis. If the inclination of the flexible domain was to be reversed during ATP synthesis, then the sharp bend 20 Å from the top of the peripheral stalk and the bend of the flexible domain would both be in the same direction.

The F_O subcomplex

The F_O portion of the map consists of two lobes, interpreted as domains. The position of the first domain, attached to the central stalk, is precisely where the c_{10}-ring is found in the atomic model of the F_1-c_{10} subcomplex from *S.cerevisiae* (Stock *et al*., 1999). The second domain, which appears to be similar in size to the c_{10} domain, is immediately adjacent to the c-ring. It extends beyond the membrane-bound portion of the complex and becomes the peripheral stalk. This domain is likely to be comprised of the membrane-bound subunits of the ATP synthase other than subunit c. These subunits include the mitochondrially encoded and hydrophobic a- and A6L-subunits (24.8 and 8.0 kDa, respectively) and possibly subunits e (8.2 kDa), f (10.2 kDa) and g (11.3 kDa) (Walker *et al*., 1991; Collinson *et al*., 1994b). As in the bacterial enzyme, there is likely to be one a-subunit per complex. The stoichiometries of subunits A6L, e, f, and g have not been determined rigorously by experiment, but they appear from intensities on stained gels to be present also in single copies. The domain probably also contains the two transmembrane helices from the peripheral stalk subunit b (Walker *et al*., 1987) which is present as a single copy in the mitochondrial complex (Collinson *et al*., 1996).

If the c-subunit exists as an oligomer of 10 copies in the bovine enzyme as it does in the *S.cerevisiae* complex (Stock *et al*., 1999), it will have a mass of 76 kDa. Two feasible extremes of subunit composition can be imagined. If the second domain contains only subunits a and A6L and 8 kDa from the two transmembrane helices from subunit b, the total mass of the domain would be ~41 kDa. If, however, it also contains subunits e, f and g, the total mass of the second domain would be 70.5 kDa. Because the second domain is nearly the same size as the c-ring domain, it appears likely that the latter case is closer to the true subunit composition. The model shows that the membrane-bound subunits other than subunit c are clustered together and not evenly distributed around the ring of c-subunits. Consequently, the contact area between the

c-ring and the domain formed by the other membrane proteins of the complex is probably quite small.

Many of the remaining structural questions about the ATP synthase can now be addressed by determining the atomic structures of appropriate subcomplexes and of individual subunits and their domains and docking them into the map that we present here.

Materials and methods

Purification of the ATP synthase from bovine heart mitochondria

Mitochondria were obtained from bovine heart tissue as described (Smith, 1967) and ATP synthase was purified chromatographically (Buchanan and Walker, 1996) in the presence of 2 mM ADP. The buffer was then exchanged to F_1F_O cryo buffer [20 mM Tris–HCl, 50 mM sucrose, 2 mM magnesium sulfate, 1 mM EDTA, 2 mM ADP, 10% (v/v) glycerol and 0.05% (w/v) Brij-35 pH 8.0] by loading onto a HiTrap Q-Sepharose column (Amersham Pharmacia Biotech, UK) and eluting with a gradient of increasing sodium chloride. The protein solution at a concentration of 3 mg/ml was stored in liquid nitrogen until use. Just before preparation of EM samples, protein solution (500 µl) was dialysed for 2 h against 1 l of F_1F_O buffer that did not contain glycerol.

Specimen preparation

Perforated carbon support films were prepared on 400-mesh copper/rhodium grids (Harris, 1962) and a thin film of protein solution (3 mg/ml) was vitrified by rapid freezing. From our experience, several experimental details were important for being able to prepare suitable specimen grids for cryoEM when using a perforated carbon support. Freezing was performed in a cold room and done with a freezing device that had a closed controlled humidity chamber (Bellare *et al*., 1988) in order to prevent concentrating the detergent and salt in the solution by evaporation. To prepare sufficiently thick ice, the grids required substantial glow-discharge treatment in air to make them hydrophilic. The result of this procedure was that the sample solution containing detergent, applied to one side of the grid, would wick through the holes in the carbon and wet both surfaces. We found that by simply blotting from one side of the grid as usual, the excess sample buffer from the opposite side of the grid was drawn back through the grid and a suitable film of amorphous ice was formed upon vitrification.

To prepare grids with a thin continuous carbon support over holes in a perforated carbon support, perforated support covered grids where placed onto a film of Formvar floating in a beaker of water. The grids and film were picked up from the water surface and a thin layer of carbon (~40 Å) was then evaporated onto the plastic layer. Finally, the Formvar was dissolved by rinsing the grids with chloroform. To render the grids hydrophilic, they were subjected to glow-discharge in air for 10 s. Protein (0.01 mg/ml) was applied, allowed to adsorb and rinsed with F_1F_O cryo buffer that did not contain detergent or glycerol. The forceps holding the grid were transferred to a freezing device, the excess buffer was removed by blotting from the side and the specimen was vitrified.

Electron microscopy and image analysis

Imaging of the ATP synthase on perforated carbon support covered grids was performed with a Tecnai F20 transmission electron microscope (FEI Company, Eindhoven, The Netherlands) equipped with a field emission gun and operating with a magnification of 50 000×, an accelerating potential of 200 kV and a defocus range of 3.5–5 µm. Vitrified specimens on a continuous carbon support were imaged with a Tecnai T12 transmission electron microscope at a magnification of 42 000×, an operating voltage of 120 kV and a defocus of ~3 µm. Both microscopes were used in a low-dose mode with samples being exposed to ~10–15 $e^-/Å^2$. Images were recorded on Kodak SO-163 film (Agar Scientific, Stansted, UK) and developed in full-strength D19 developer solution for 12 min.

Micrographs were digitized with a Zeiss SCAI scanner (Carl Zeiss Ltd, Oberkochen, Germany) with the step size set at 7 µm. Averaging over 2 × 2 pixels was performed to give an effective pixel size of 14 × 14 µm (2.8 Å at the specimen).

Particle selection, windowing and floating were done with the MRC image analysis software suite (Crowther *et al*., 1996). Multireference alignment (MRA) and multivariate statistical analysis (MSA) for the purpose of image classification were done using the program IMAGIC (van Heel *et al*., 1996). A new Fortran 90 program (ROTAN) was written to fit the marker positions in Figure 3A to a rotation model. Values of ϕ for each image, and δ and r for each marker were calculated by using 1 million random starts of an implementation of the conjugate gradient method (Press *et al*., 1986) to minimize the error function

$$f = \sum_{i=1}^{m}\sum_{j=1}^{n}(r_i \cos(\phi_j + \delta_i) - a_{i,j})^2$$

where $a_{i,j}$ is the measured position of the ith of m markers in the jth of n images. The 'movie' was prepared using Adobe Image Ready (San Jose, CA, USA).

The angles determined by ROTAN were used by FREALIGN (Grigorieff, 1998) to build the initial 3-D model of the complex. Projections from the model with Eulerian rotations $\phi = 0$–$360°$ in steps of 15° and $\theta = 60$–$120°$ in steps of 15° were then produced by FREALIGN. The projections were used as references for MRA of all of the particle images and the images were then reclassified into 100 classes. Projection matching of the class-averages was performed with FREALIGN version 5.03 modified so that the initial search of orientations was limited to $85 < \theta < 95°$ but could be refined to any orientation by the Powell minimizer subroutine. Orientation parameters were determined by randomized search and refinement (IFLAG = –4, DANG = 200°) with 200 random starts per class (ITMAX = 200). The particle radius (RI) was set to 120 Å and the model was masked at 1 standard deviation above the mean (XSTD = –1.0). The search was conducted in the resolution range 120 Å (RMAX1) to 40 Å (RMAX2). Because CTF correction was done after determining class-orientations, the value of the CTF was set to –1.0 during alignment (WGH = –1.0, Cs = 0, defocus = 0).

The process of alignment and map building was iterated six times. A new set of projections was generated from the model and used as references for MRA of all 5984 particle images. Particle images were subjected to MSA and the classes were again aligned to the model until the image orientations stabilized (five iterations). The CTF parameters for each film were determined using CTFFIND2. A program was written (CTFCORRECT_CLASS) in order to weight the structure factors in each class-average as

$$F_{class-average}(h,k) = \frac{\sum_{j=1}^{n} CTF_j(h,k) \cdot F_j(h,k)}{\sum_{j=1}^{n} CTF_j(h,k)^2}$$

where n is the number of particles in a particular class and $CTF(h,k)$ describes the contrast transfer function of the microscope (Wade, 1992). A phase residual threshold (THRESH) was set so that only the 64 best CTF-corrected class-averages (containing 3665 particle images) were included in the final model. The experimental map was divided into two segments by masking sections of the density with IMAGIC to separate the F_1-c_{10} region from the peripheral stalk and second domain of F_O.

Using the program O (Jones *et al*., 1991), the F_1-c_{10} model was assembled from the bovine F_1-ATPase structure 1E79 (Gibbons *et al*, 2000) and the *E.coli* c-subunit structure 1A91 (Girvin *et al*., 1998) modelled into an oligomer of 10 copies in 1QO1 (Stock *et al*., 1999). The F_1-c_{10} model was manually docked into the EM map with O. Figures 4, 5 and 7 were prepared with AESOP (M.Noble, unpublished).

A pair of low-dose images recorded from the same area of the specimen but differing by a relative tilt angle of 30° (a counter-clockwise rotation when viewed along the specimen holder from the nitrogen Dewar to the holder tip) was used to determine the absolute hand of the 3-D model (Rosenthal and Henderson, 2003).

Supplementary data

Supplementary data are available at *The EMBO Journal* Online.

Acknowledgements

We thank Dr P.B.Rosenthal for advice and Dr G.J.Mitchison for discussions and help with writing ROTAN. Drs D.Stock and A.G.W.Leslie are gratefully acknowledged for discussions about docking the F_1-c_{10} structure.

References

Abrahams,J.P., Leslie,A.G., Lutter,R. and Walker,J.E. (1994) Structure at 2.8 Å resolution of F_1-ATPase from bovine heart mitochondria. *Nature*, **370**, 621–628.

Bellare,J.R., Davis H.T., Scriven,L.E. and Talmon,Y. (1988) Controlled environment vitrification system: an improved sample preparation technique. *J. Electron Microsc. Tech.*, **10**, 87–111.

Böttcher,B., Schwarz,L. and Gräber,P. (1998) Direct indication for the existence of a double stalk in CF_oF_1. *J. Mol. Biol.*, **281**, 757–762.

Böttcher,B., Bertsche,I., Reuter,R. and Gräber,P. (2000) Direct visualisation of conformational changes in EF_OF_1 by electron microscopy. *J. Mol. Biol.*, **296**, 449–457.

Boyer,P.D. (1997) The ATP synthase—a splendid molecular machine. *Annu. Rev. Biochem.*, **66**, 717–749.

Buchanan,S.K. and Walker,J.E. (1996) Large-scale chromatographic purification of F_1F_O-ATPase and complex I from bovine heart mitochondria. *Biochem. J.* **318**, 343–349.

Cabezón,E., Runswick,M.J., Leslie,A.G. and Walker,J.E. (2001) The structure of bovine IF1, the regulatory subunit of mitochondrial F-ATPase. *EMBO J.*, **20**, 6990–6996.

Cabezón,E., Montgomery,M.G., Leslie,A.G.W.L. and Walker,J.E. (2003) The structure of bovine F_1-ATPase complexed with its regulatory protein, IF_1. *Nat. Struct. Biol.*, **10**, 744–750.

Cherepanov,D.A., Mulkidjanian,A.Y. and Junge,W. (1999) Transient accumulation of elastic energy in proton translocating ATP synthase. *FEBS Lett.*, **449**, 1–6.

Collinson,I.R., van Raaij,M.J., Runswick,M.J., Fearnley,I.M., Skehel,J.M., Orriss,G.L., Miroux,B. and Walker,J.E. (1994a) ATP synthase from bovine heart mitochondria. *In vitro* assembly of a stalk complex in the presence of F_1-ATPase and in its absence. *J. Mol. Biol.*, **242**, 408–421.

Collinson,I.R., Runswick,M.J., Buchanan,S.K., Fearnley,I.M., Skehel,J.M., van Raaij,M.J., Griffiths,D.E. and Walker,J.E. (1994b) F_O membrane domain of ATP synthase from bovine heart mitochondria: purification, subunit composition and reconstitution with F_1-ATPase. *Biochemistry*, **33**, 7971–7978.

Collinson,I.R., Skehel,J.M., Fearnley,I.M., Runswick,M.J. and Walker,J.E. (1996) The F_1F_O-ATPase complex from bovine heart mitochondria: the molar ratio of the subunits in the stalk region linking the F_1 and F_O domains. *Biochemistry*, **35**, 12640–12646.

Crowther,R.A., Amos,L.A., Finch,J.T., De Rosier,D.J. and Klug,A. (1970) Three dimensional reconstructions of spherical viruses by Fourier synthesis from electron micrographs. *Nature*, **226**, 421–425.

Crowther,R.A., Henderson,R. and Smith,J.M. (1996) MRC image processing programs. *J. Struct. Biol.*, **116**, 9–16.

Del Rizzo,P.A., Bi,Y., Dunn,S.D. and Shilton,B.H. (2002) The 'second stalk' of *Escherichia coli* ATP synthase: structure of the isolated dimerization domain. *Biochemistry*, **41**, 6875–6884.

Dmitriev,O., Jones,P.C., Jiang,W. and Fillingame,R.H. (1999) Structure of the membrane domain of subunit b of the *Escherichia coli* F_OF_1 ATP synthase. *J. Biol. Chem.*, **274**, 15598–15604.

Dupuis,A. and Vignais,P.V. (1985) Photolabelling of mitochondrial F_1-ATPase by an azido derivative of the oligomycin-sensitivity conferral protein. *Biochem. Biophys. Res. Commun.*, **129**, 819–825.

Gibbons,C., Montgomery,M.G., Leslie,A.G. and Walker,J.E. (2000) The structure of the central stalk in bovine F_1-ATPase at 2.4 Å resolution. *Nat. Struct. Biol.*, **7**, 1055–1061.

Girvin,M.E., Rastogi,V.K., Abildgaard,F., Markley,J.L. and Fillingame,R.H. (1998) Solution structure of the transmembrane H^+-transporting subunit c of the F_1F_O ATP synthase. *Biochemistry*, **37**, 8817–8824.

Grabar,T.B. and Cain,B.D. (2003) Integration of b subunits of unequal lengths into F_1F_O ATP synthase. *J. Biol. Chem.*, **37**, 34751–34756.

Grigorieff,N. (1998) Three-dimensional structure of bovine NADH:ubiquinone oxidoreductase (complex I) at 22 Å in ice. *J. Mol. Biol.*, **277**, 1033–1046.

Groth,G. and Pohl,E. (2001) The structure of the chloroplast F_1-ATPase at 3.2 Å resolution. *J. Biol. Chem.*, **276**, 1345–1352.

Harris,J.W. (1962) Holey films for electron microscopy. *Nature*, **196**, 499–500.

Hundal,T., Norling,B. and Ernster,L. (1983) Lack of ability of trypsin-treated mitochondrial F_1-ATPase to bind the oligomycin-sensitivity conferring protein (OSCP). *FEBS Lett.*, **162**, 5–10.

Jones,T.A., Zou,J.Y., Cowan,S.W. and Kjeldgaard,M. (1991) Improved methods for binding protein models in electron density maps and the location of errors in these models. *Acta Crystallogr. A*, **47**, 110–119.

Joshi,S., Cao,G.J., Nath,C. and Shah,J. (1996) Oligomycin sensitivity conferring protein of mitochondrial ATP synthase: deletions in the N-terminal end cause defects in interactions with F1, while deletions in the C-terminal end cause defects in interactions with F_O. *Biochemistry*, **35**, 12094–12103.

Junge,W., Lill,H. and Engelbrecht,S. (1997) ATP synthase: an electrochemical transducer with rotatory mechanics. *Trends Biochem. Sci.*, **22**, 420–423.

Karrasch,S. and Walker,J.E. (1999) Novel features in the structure of bovine ATP synthase. *J. Mol. Biol.*, **290**, 379–384.

Ma,J., Flynn,T.C., Cui,Q., Leslie,A.G.W., Walker,J.E. and Karlplus,M. (2002) A dynamic analysis of the rotation mechanism for conformational change in F_1-ATPase. *Structure*, **10**, 921–931.

McLachlin,D.T., Coveny,A.M., Clark,S.M. and Dunn,S.D. (2000) Site-directed cross-linking of b to the α, β and a subunits of the *Escherichia coli* ATP synthase. *J. Biol. Chem.*, **275**, 17571–17577.

Mellwig,C. and Böttcher,B. (2001) Dealing with particles in different conformational states by electron microscopy and image processing. *J. Struct. Biol.*, **133**, 214–220.

Mellwig,C. and Böttcher,B. (2003) A unique resting position of the ATP-synthase from chloroplasts. *J. Biol. Chem.*, **278**, 18544–18549.

Noji,H., Yasuda,R., Yoshida,M. and Kinosita,K.,Jr (1997) Direct observation of the rotation of F_1-ATPase. *Nature*, **386**, 299–302.

Ogilvie,I., Aggeler,R. and Capaldi,R.A. (1997) Cross-linking of the δ subunit to one of the three α subunits has no effect on functioning, as expected if δ is a part of the stator that links the F_1 and F_O parts of the *Escherichia coli* ATP synthase. *J. Biol. Chem.*, **272**, 16652–16656.

Pänke,O., Gumbiowski,K., Junge,W. and Engelbrecht,S. (2000) F-ATPase: specific observation of the rotating c subunit oligomer of EF_OEF_1. *FEBS Lett.*, **472**, 34–38.

Press,W.H., Flannery,B.P., Teukolsky,S.A. and Vetterling,W.T. (1986) *Numerical Recipes: the Art of Scientific Computing*. Cambridge University Press, Cambridge, UK, pp. 305–306.

Rosenthal,R.B. and Henderson,R. (2003) Optimal determination of particle orientation, absolute hand and contrast loss in single-particle electron microscopy (Appendix). *J. Mol. Biol.*, **333**, 721–742.

Rosenthal,P.B., Crowther,A.C. and Henderson,R. (2003) An objective criterion for resolution assessment in single-particle electron microscopy (Appendix). *J. Mol. Biol.*, **333**, 743–745.

Rubinstein,J.L. and Walker,J.E. (2002) ATP Synthase from *Saccharomyces cerevisiae*: location of the OSCP subunit in the peripheral stalk region. *J. Mol. Biol.*, **321**, 613–619.

Sambongi,Y., Iko,Y., Tanabe,M., Omote,H., Iwamoto-Kihara,A., Ueda,I., Yanagida,T., Wada,Y. and Futai,M. (1999) Mechanical rotation of the c subunit oligomer in ATP synthase (F_OF_1): direct observation. *Science*, **286**, 1722–1724.

Seelert,H., Poetsch,A., Dencher,N.A., Engel,A., Stahlberg,H. and Muller,D.J. (2000) Proton-powered turbine of a plant motor. *Nature*, **405**, 418–419.

Sigworth,F.J. (1998) A maximum-likelihood approach to single-particle image refinement. *J. Struct. Biol.* **122**, 328–339.

Smith,A.L. (1967) Preparation, properties and conditions for assay of mitochondria: slaughterhouse material, small-scale. *Methods Enzymol.*, **10**, 81–86.

Sorgen,P.L., Caviston,T.L., Perry,R.C. and Cain,B.D. (1998) Deletions in the second stalk of F_1F_O-ATP synthase in *Escherichia coli*. *J. Biol. Chem.*, **273**, 27873–27878.

Sorgen,P.L., Bubb,M.R. and Cain,B.D. (1999) Lengthening the second stalk of F_1F_O ATP synthase in *Escherichia coli*. *J. Biol. Chem.*, **274**, 36261–36266.

Stahlberg,H., Muller,D.J., Suda,K., Fotiadis,D., Engel,A., Meier,T., Matthey,U. and Dimroth,P. (2001) Bacterial Na^+-ATP synthase has an undecameric rotor. *EMBO Rep.*, **2**, 229–233.

Stock,D., Leslie,A.G. and Walker,J.E. (1999) Molecular architecture of the rotary motor in ATP synthase. *Science*, **286**, 1700–1705.

van Heel,M. (1987) Angular reconstitution: a posteriori assignment of projection directions for 3D reconstruction. *Ultramicroscopy*, **21**, 111–124.

van Heel,M., Harauz,G. and Orlova,E.V. (1996) A new generation of the IMAGIC image processing system. *J. Struct. Biol.*, **116**, 17–24.

Wade,R.H. (1992) A brief look at imaging and contrast transfer. *Ultramicroscopy*, **46**, 145–156.

Walker,J.E. (1998) ATP synthesis by rotary catalysis (Nobel lecture). *Angew. Chem. Int. Ed.*, **37**, 2308–2319.

Walker,J.E., Fearnley,I.M., Gay,N.J., Gibson,B.W., Northrop,F.D.,

Powell,S.J., Runswick,M.J., Saraste,M. and Tybulewicz,V.L. (1985) Primary structure and subunit stoichiometry of F_1-ATPase from bovine mitochondria. *J. Mol. Biol.*, **184**, 677–701.

Walker,J.E., Runswick,M.J. and Poulter,L. (1987) ATP synthase from bovine mitochondria. The characterization and sequence analysis of two membrane-associated sub-units and of the corresponding cDNAs. *J. Mol. Biol.*, **197**, 89–100.

Walker,J.E., Lutter,R., Dupuis,A. and Runswick,M.J. (1991) Identification of the subunits of F_1F_O-ATPase from bovine heart mitochondria. *Biochemistry*, **30**, 5369–5378.

Wilkins,S. (2000) F_1F_O-ATP synthase—stalking mind and imagination. *J. Bioeneg. Biomemb.*, **32**, 333–339.

Wilkens,S. and Capaldi,R.A. (1998a) ATP synthase's second stalk comes into focus. *Nature*, **393**, 29.

Wilkens,S. and Capaldi,R.A. (1998b) Electron microscopic evidence of two stalks linking the F_1 and F_O parts of the *Escherichia coli* ATP synthase. *Biochim. Biophys. Acta*, **1365**, 93–97.

Wilkens,S., Dunn,S.D., Chandler,J., Dahlquist,F.W. and Capaldi,R.A. (1997) Solution structure of the N-terminal domain of the δ subunit of the *E. coli* ATP synthase. *Nat. Struct. Biol.*, **4**, 198–201.

Received August 28, 2003; revised October 9, 2003; accepted October 13, 2003